4 RESULTS

4.1 Comparison of OPA1 splice variants in different mouse tissues.

Mutations in the OPA1 gene specifically cause the loss of retinal ganglion cells (RGC) that leads to an atrophy of the optic nerve in patients affected with autosomal dominant optic atrophy. Although the disease affects only the optic nerve, OPA1 is ubiquitously expressed in all tissues. Delettre and co-workers (2001 and 2003) reported the presence of eight different OPA1 mRNA transcripts in humans and mice generated by alternative splicing involving exons 4, 4b and 5b. On western blots, mouse retina and brain protein extracts displayed identical OPA1 expression patterns, which differed from the ones observed in other organ tissues. Therefore, this part of the study was focussed on identifying tissue specific features of OPA1 mRNA transcripts by comparing their expression in the mouse brain with other tissues.

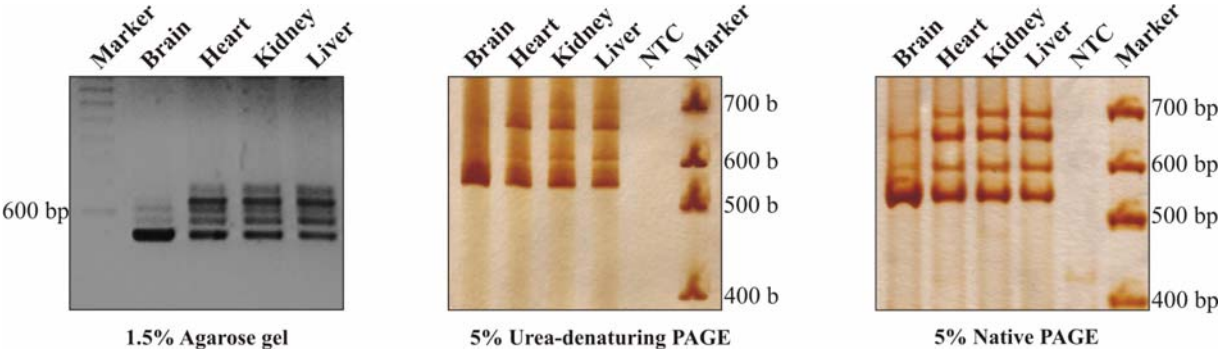

Figure 4.1: Analysis of RT-PCR product obtained from primer pair 3-9.

Total RNA was isolated from mouse tissues (brain, heart, liver and kidney; Chapter 3.2) and reverse transcribed (Chapter 3.3). Using specific primers located in exons 3 and 9 (Table 4.1a, b), the region encompassing all the alternatively spliced exons was amplified by PCR and analysed by agarose gel electrophoresis (AGE). Five PCR fragments in the expected size range were observed in the heart, liver and kidney, whereas in the brain only four fragments were detected when analysed on a 1.5% AGE (Fig. 4.1). Since the number of the observed bands did not correspond to the expected number of splice variants, all bands were cut out from the gels, eluted and sequenced. The identity of the shortest band was confirmed as a splice form 1 consisting of exons 3/4/5/6. All the other bands contained mixtures of splice forms 1, 5, 7 and 8 (data not shown). These splice forms contained exon 4, but differed in the presence of exons 4b and 5b. At this stage, a discrepancy with the data published by Delettre and co-workers (eight splice variants) became apparent and the search for OPA1 transcripts, that did not contain exon 4, was carried out.

In order to separate the homogeneous products of single splice variants, native and denaturing polyacrylamide gel electrophoresis (PAGE) was applied. The power of separation of PAGE is much higher than that of agarose gel electrophoresis. The same RT-PCR reaction generated by primers 3 and 9 was loaded on the high-resolution 5% PAGE. Silver staining clearly revealed only four products ranging from 500 bp to 700 bp (Fig. 4.1). The longest fragment (698 bp) was amplified from splice form 8 and the 644 bp fragment was generated from splice form 7. The identity of the two other bands (~ 540 bp and ~ 590 bp) remained undefined using this method. The reason for this is that the theoretical fragments amplified from splice forms 1 (533 bp) and 4 (536 bp), as well as 5 (587 bp) and 6 (590 bp) differed only 3 bp in length. However, splice forms 2 and 3 were never detected by either sequencing or gel electrophoresis.

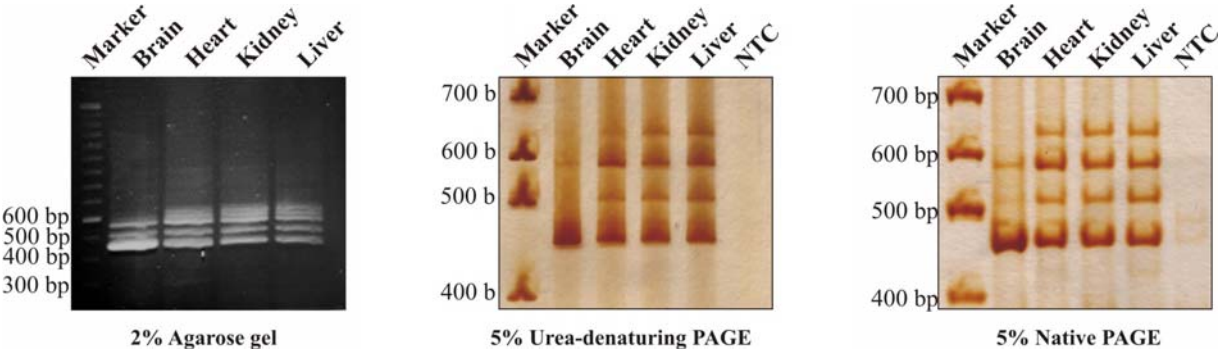

Figure 4.2: Analysis of RT-PCR product obtained from primer pair 4-9.

The existence of splice forms 1 and 5 was apparent from the sequencing data. In order to visualise the presence of these splice forms in the gel, the primer pair 4-9 was used which specifically amplified splice forms that contained exon 4 (Table 4.1b). Figure 4.2 shows the analysis of the RT-PCR product on 2% AGE and by 5% PAGE. Four fragments in the brain and five fragments in other tissues with sizes ranging from 400 bp to 700 bp were observed in AGE (Fig. 4.2). Sequencing of these fragments from agarose gels together with PAGE analysis confirmed that the longest fragment resulted from splice form 8 (623 bp), followed by splice form 7 (569 bp), splice form 5 (512 bp) and splice form 1 (458 bp) (Fig. 4.2). Therefore, the presence of splice forms 1 and 5 in the mouse tissues was confirmed.

Splice forms 4 and 6 contain exon 5b (111 bp insert between exon 5 and exon 6), whereas it is not present in the splice forms 1 and 5. A combination of two PCR reactions was performed, in order to specifically amplify splice forms harbouring exon 5b. The first reaction was run with primer pair 3-9, to increase the template concentration for the second PCR, which was a nested PCR run with primer pair 3-5b (Table 4.1b).

Table 4.1a: Details of primers used for the amplification of splice forms of OPA1

Primer pair	Forward primer	Reverse primer	Starting exon	Ending exon	Annealing temperature
3-9	CTA TAA GTG GAT TGT GCC TGA	GCA ATC ATT TCC AGC ACA CTG	3	9	62°C
4-9	GCC CAG CTC AGA AGA CCT	GCA ATC ATT TCC AGC ACA CTG	4	9	64°C
4-5b	GCC CAG CTC AGA AGA CCT	TCT GCG TGC TTC CTC TTC	4	5b	60°C
3-5b (nested from 3-9)	CTA TAA GTG GAT TGT GCC TGA	TCT GCG TGC TTC CTC TTC	3	5b	60°C
e3-e7	GTG ACT ATA AGT GGA TTG TGC CT	CGC TCC AAG ATC CTC TGA TAC	3	7	62°C

Table 4.1b: Details of the expected lengths of PCR products generated using specific primers.

Splice forms	Spliced exon	3-9	4-9	3-5b (nested from 3-9)	e3-e7	4-5b
Splice form 8 (3/4/4b/5/5b/6)	--	698 bp	623 bp	351	480	276 bp
Splice form 7 (3/4/5/5b/6)	Δ exon 4b	644 bp	569 bp	297	426	222 bp
Splice form 6 (3/4b/5/5b/6)	Δ exon 4	590 bp	**	243	372	**
Splice form 5 (3/4/4b/5/6)	Δ exon 5b	587 bp	512 bp	**	369	**
Splice form 4 (3/5/5b/6)	Δ exon 4, 4b	536 bp	**	189	318	**
Splice form 1 (3/4/5/6)	Δ exon 4b, 5b	533 bp	458 bp	**	315	**
Splice form 3 (3/4b/5/6)	Δ exon 4, 5b	479 bp	**	**	261	**
Splice form 2 (3/5/6)	Δ exon 4, 4b, 5b	425 bp	**	**	207	**

** Cannot be detected

Two fragments of sizes ranging from 300 bp to 400 bp were detected on a 3% agarose gel (Fig. 4.3). PAGE analysis and sequencing of agarose-gel eluted fragments confirmed the existence of the longest fragment (351 bp) as a splice form 8 and the shortest fragment (297 bp) as a splice form 7. This indicates that splice forms 4 and 6 are not present in the analysed mouse tissues.

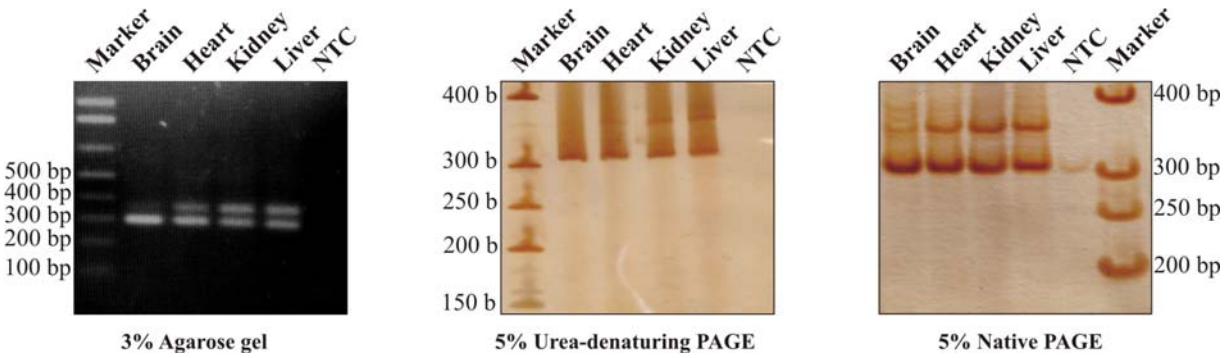

Figure 4.3: Analysis of RT-PCR product obtained from primer pair 3-5b.

Finally, the described results were compared to the products observed in a reaction using the published conditions (Delettre et al., 2003). Only splice form 8 (480 bp), splice form 7 (426 bp), splice form 5 (369 bp) and splice form 1 (315 bp) were detected by sequencing and size comparison on PAGE (Fig. 4.4).

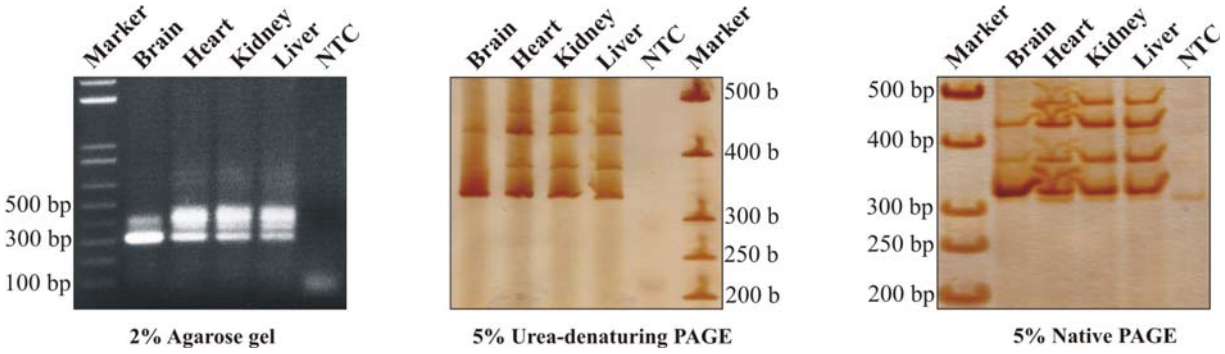

Figure 4.4: Analysis of RT-PCR product obtained from primer pair e3-e7 (Table 4.1a).

In summary, the presence of mRNA transcripts from the splice forms 1, 5, 7 and 8, which results from alternative splicing involving exons 4b and 5b, was demonstrated in the mouse tissues. mRNA transcripts of splice variants 2, 3, 4 and 6, which would result from an additional alternative splicing of exon 4 were not detected.

4.1.1 Expression profile of OPA1 splice forms in mouse.

The above studies clearly indicate the absence of any nerve tissue specific splice variant in the mouse. To further examine the tissue specific differences in OPA1 gene expression, the obtained data were examined for individual transcript abundance in the studied tissues. This

was done under the assumption that the PCR amplification level is directly proportional to the template concentration. Of note here is that the amplification profile of the OPA1 splice forms in each tissue did not vary with changing the annealing temperature during the PCR reaction. However, the total product yield was reduced under non-optimal annealing conditions, indicating that the amplification of specific splice forms was independent of the annealing temperature (data not shown).

Table 4.2: Expression profile of OPA1 splice forms.

Splice forms	Brain	Heart	Liver	Kidney
1	+++++	++++	++++	++++
5	+	++	++	++
7	++	+++	+++	+++
8	+	++	++	++

The individual amount of transcript for splice variants 1, 5, 7, and 8 was similar in the heart, kidney and liver. Isoforms 1 and 7 were always found to be more abundant than splice forms 5 and 8 (Table 4.2). In contrast, the level of individual splice forms in the brain tissue significantly differed from ones observed in the heart, kidney and liver. Transcripts from splice form 1 showed very high level of expression compared to the other splice forms in the brain. Splice form 7 was expressed at moderate level, but present in higher abundance than splice form 5. Amplification products of splice form 8 were not visible in the PAGE analysis (Fig. 4.1).

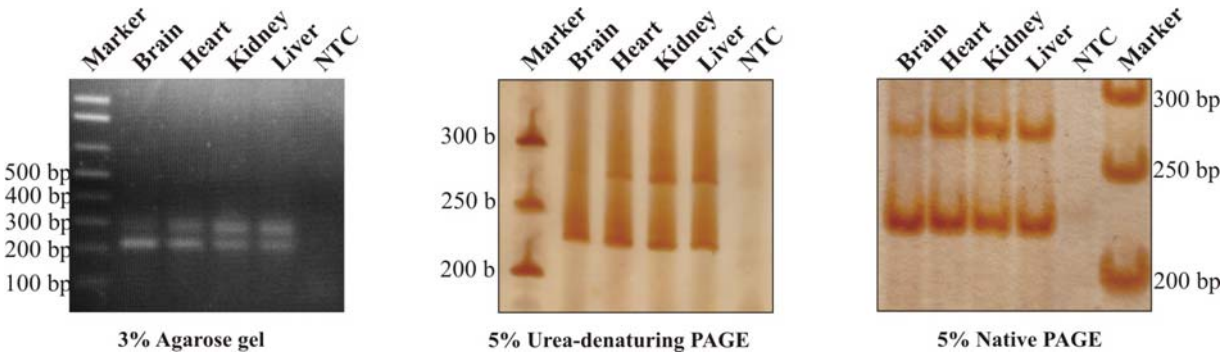

Figure 4.5: Analysis of RT-PCR product obtained from primer pair 4-5b.

In order to prove the existence of splice form 8 in the brain tissue, primer pair 4-5b was applied. This primer pair specifically amplified only two products (Fig. 4.5). These fragments were confirmed as splice forms 8 (276 bp) and 7 (222 bp), by sequencing and PAGE.

4.2 Comparative study of OPA1 protein expression in different tissues

4.2.1 Generation of anti-OPA1 monoclonal antibodies

In order to characterize the OPA1 protein expression in different tissues, monoclonal antibodies were generated. The region corresponding to the amino acids 111-960 of human OPA1 isoform 1 was PCR amplified with specific primer pairs from the source clone 3F-1R-pCDNA and TA-cloned into the pGEMT-Easy vector. The correct insert was confirmed by restriction enzyme digest and sequencing. Restriction cloning was used to subclone the insert into the pGEX-2T vector in order to generate a GST-fusion protein (Fig. 4.6). Since OPA1 fusion protein was expressed in an insoluble form in *E. coli*, it was electroeluted from SDS-PAGE gels and the protein was dialysed against PBS. After centrifugation, the soluble protein fraction was used as an antigen for the production of monoclonal antibodies.

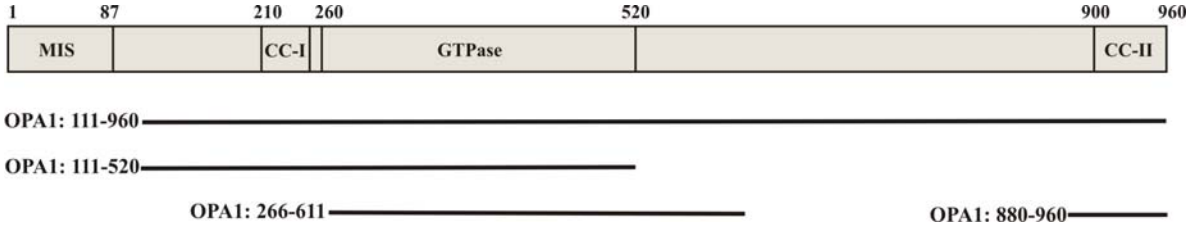

Figure 4.6: Schematic representation of the regions amplified for the antibody characterization.
The numbers assigned to the clone name represent the amino acid position corresponding to the human OPA1 ORF isoform 1.

Six hybridoma clones were judged as positive after ELISA screening against the antigen (1A8, 2A4, 2F12, 3H5, 2E5 and 1D4).

4.2.1.1 Epitope mapping of the OPA1 monoclonal antibodies

In order to map the epitope region recognised by the six monoclonal antibodies, a set of OPA1 fusion constructs were generated using the method described above, representing the different domains of the OPA1 protein and expressed in *E. coli* (Fig. 4.6). The *OPA1: 111-520* fragment was generated as a GST-fusion, *OPA1: 880-960* fragment as a Nus-fusion (Chapter 4.2), while *OPA1: 266-611* was expressed as a His_6-fusion protein (gift by Anita Bulczak). High expression levels were observed for all the clones albeit with the low solubility, except for the fragment *OPA1: 880-960*. The details of the primers, vectors and restriction sites used for sub-cloning are provided in Chapter 7.3. In order to individually map the epitope recognised by each of the OPA1-positive hybridomas, the library of fusion proteins *OPA1: 111-960*, *OPA1: 111-520*, *OPA1: 266-611* and *OPA1: 880-960* (Nus-CCII) was systematically screened by western blotting (Fig. 4.7a, b).

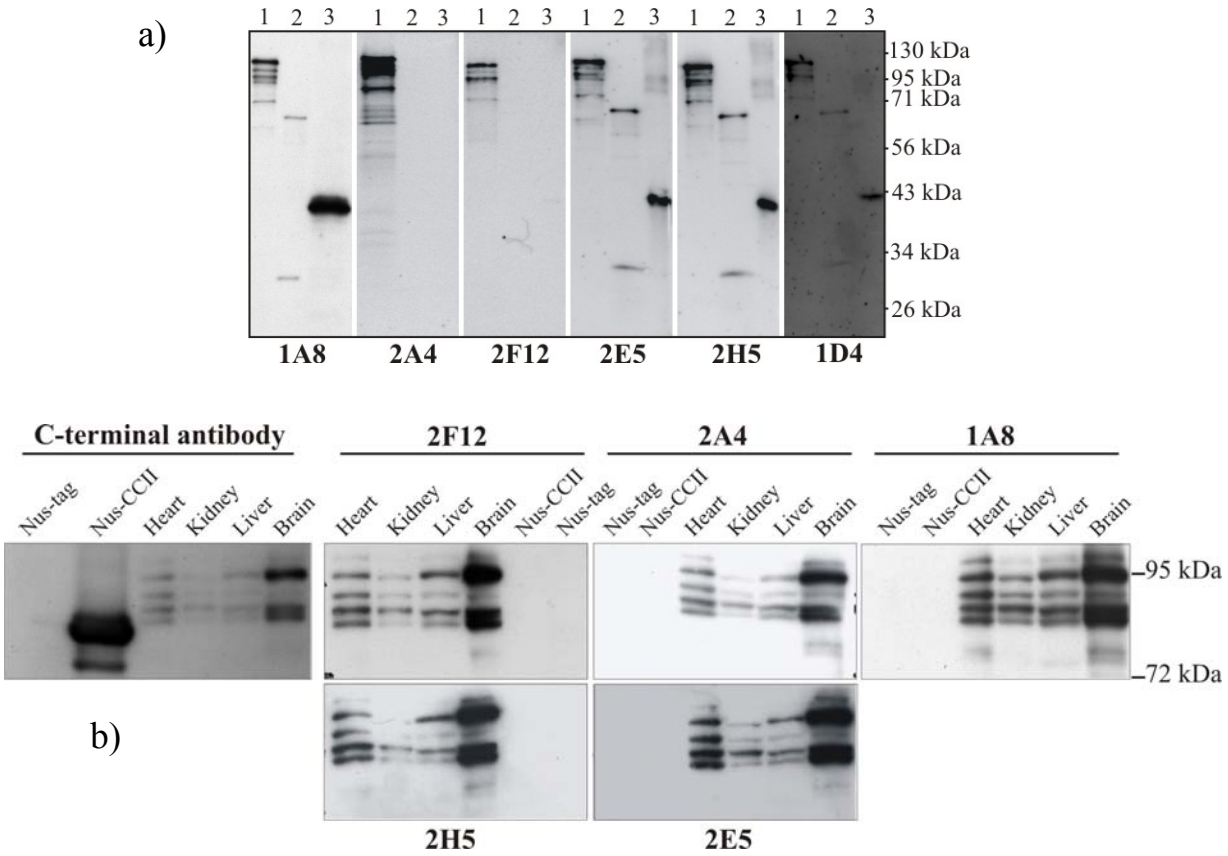

Figure 4.7: Epitope mapping of the hybridomas.

a) The hybridoma clones were screened by western blotting against three different fusion proteins expressed in E.coli: 1 (*OPA1: 111-960* -125kDa); 2 (*OPA1: 111-520* – 72kDa); 3 (*OPA1: 266-611* –39kDa).

b) Western blots demonstrating specificity of OPA1 antibodies. The C-terminal antibody (positive control) recognised the *OPA1: 880-960* (Nus-CC-II - 72-kDa) protein specifically, whereas none of the hybridomas recognised this fusion protein indicating that the epitope for these clones lies outside the CC-II region. All antibodies recognised OPA1 in mouse mitochondrial lysates from heart, kidney, liver, and brain tissues.

The six OPA1-positive hybridoma cell lines were grouped according to the epitope mapping results. Clones 1A8, 2E5, 2H5, and 1D4 recognised the GTPase domain of OPA1 (aa 266-520), while clones 2A4 and 2F12 detected the middle domain (aa 611-880). None of the hybridoma clones cross-reacted with the GST tag (data not shown) or Nus-tag (Fig. 4.7b).

Table 4.3: Epitope mapping of the hybridomas that recognised OPA1

Clone number	OPA1: 111-960	OPA1: 111-520	OPA1 266-611	Nus-CC-II	Epitope region (aa position)
1A8	+	+	+	-	266-520
2A4	+	-	-	-	611-880
2F12	+	-	-	-	611-880
2E5	+	+	+	-	266-520
2H5	+	+	+	-	266-520
1D4	+	+	+	-	266-520

(+) protein of proper molecular weight is recognised; (-)not recognised in western blots.

A summary of the epitope mapping results is given in the Table 4.3. The antibody titre for each hybridoma clone was determined using ELISA. The clone 1A8, which showed the

highest titre, was used for the production of ascites fluid and then applied at a 1:5000 dilution in western blotting experiments. This antibody cross-reacted with mouse OPA1 (Fig. 4.7b) and rat OPA1, but did not react with Drosophila OPA1 (data not shown).

4.2.1.2 Specificity of anti-OPA1 antibodies

In order to confirm the specificity of the monoclonal antibodies for endogenously expressed OPA1, the hybridoma supernatants were tested on mitochondrial isolates from different mouse tissues by western blotting. All antibodies detected a set of five OPA1 isoforms in the molecular weight range of 72-kDa to 95-kDa. A positive control antibody (gift by Andreas Reichert; Duvezin-Caubet et al., 2006) recognised the same set of OPA1 isoforms (Fig. 4.7b). Due to its very low antibody titre, clone 1D4 was not used in the experiments.

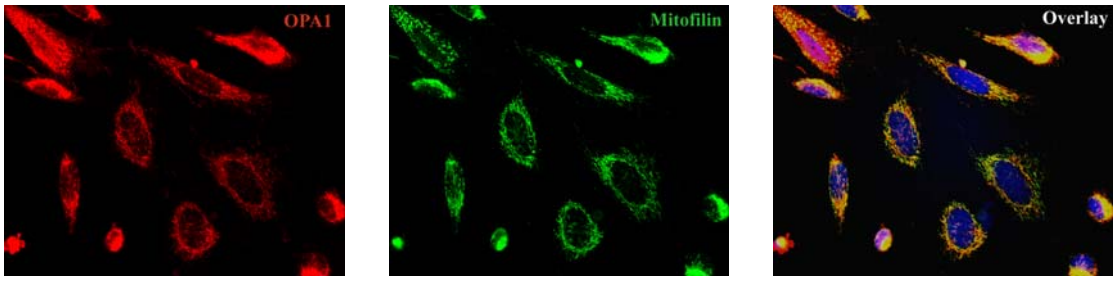

Figure 4.8: Mitochondrial localisation of OPA1 in HeLa cells.
Anti-OPA1 (Clone 1A8) monoclonal antibody (1:500) specifically recognised OPA1 (red) in the mitochondria. Anti-mitofilin antibody (gift by Odgren Paul -1:1000) was used as positive control (green), as mitofilin is localised to the inter membrane space for mitochondria (Odgren et al., 1996).

OPA1 is a mitochondrial protein imported into the mitochondria via its N-terminal import sequence. For this reason, immunostaining on the HeLa cells was performed to confirm the mitochondrial localisation of OPA1. The anti-OPA1 monoclonal antibody (clone 1A8) revealed a typical tubular mitochondrial network in HeLa cells, which perfectly overlapped with the anti-mitofilin antibody signal (John et al., 2005). Mitofilin is also an intermembrane space mitochondrial protein (Fig. 4.8). Identical staining patterns were observed with all other OPA1 hybridoma supernatants (data not shown). This result is in agreement with the finding that OPA1 was localised in the mitochondria tightly bound to the inner membrane (Satoh et al, 2003).

4.2.2 Expression profile of the OPA1 protein as detected by OPA1 antibody

In the mouse OPA1 transcript analysis, tissue specific splice variants were not identified, however, splice variant 1 was predominantly expressed in the brain. In order to decipher how the particular OPA1 transcript composition in nerve tissue translates into specific protein pattern, OPA1 protein isoforms were examined in detail. To achieve it, protein isolates were

separated by high resolution, 18 cm long, SDS-PAGE (8%) gels, blotted and detected using anti-OPA1 monoclonal antibody. Although the antibody did not recognize any tissue specific OPA1 isoforms in mouse and human samples, the relative abundance of individual OPA1 isoforms differed for each tissue studied (Fig. 4.9).

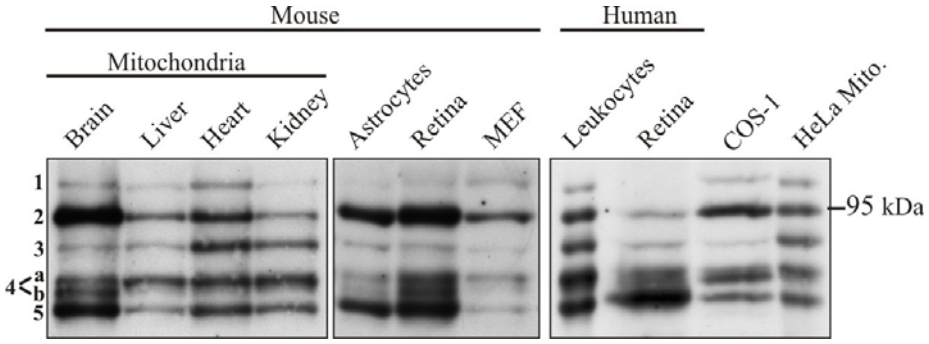

Figure 4.9: Expression profile of various OPA1 protein forms from mouse and human.

Western blot analysis of mouse- mitochondrial lysates from the brain (15 µg), liver (60 µg), heart (27 µg) and kidney (34 µg); total protein lysates from astrocyte primary cell line, retina and mouse embryonic fibroblasts (MEF). Total protein lysates from human leukocyte cell lines and retina, COS-1 cells and mitochondrial lysates from HeLa cells as detected by α-OPA1 monoclonal antibody.

Apart from the five previously observed OPA1 protein bands (Fig. 4.7b), an additional sixth band was clearly visible after high-resolution PAGE (band-4b in Fig. 4.9). This band was present in all analysed lysates, albeit at low abundance. In the lysates isolated from the mouse nervous system, e.g. brain, retina, and astrocytes, the distribution and immunoreactivity of different bands was comparable. The intensity of band-2 was the highest among the OPA1 bands, while band-5 displayed a moderate level of expression. Also in embryonic fibroblasts, high signal intensity was observed for band-2. In mouse heart, all OPA1 forms were equally abundant except for protein band-1. In mouse liver and kidney, the protein band-4a was strongly expressed (Fig. 4.9).

Table 4.4: Expression profile of OPA1 protein forms

Tissue / cells	Band 1	Band 2	Band 3	Band 4a	Band 4b	Band 5
Mouse						
Brain	++	+++++	++	+++	+++	++++
Liver	+	++++	+++	+++++	++	+++
Heart	++	+++++	+++++	+++++	+	+++++
Kidney	+	+++	++++	+++++	++	++++
Astrocytes	++	+++++	++	+++	+++	++++
Mouse retina	++	+++++	++	+++	+++	++++
MEF	++	+++++	+	+++	+	++
Human						
Leukocytes	++	+++++	+++++	+++++	+++++	+++++
Human retina	+	+++	++	++++	++++	+++++
COS-1	+	+++++	+	++	++++	++
HeLa	+++	+++++	+++++	+++++	++	+++++

"+++++" Indicates the relative predominance and "+" relative least abundance in a particular tissue/cell lysates

The OPA1 band-2 in the human retina was reduced in its abundance in comparison to the mouse retina. In human cell lines, e.g. HeLa cells and immortalised lymphoblasts, the expression profile of OPA1 protein forms was comparable to that of the mouse heart. In COS-1 cells, the protein band-2 was mostly visible followed by bands-4b and -5, with moderate signal intensity (Fig. 4.9). The expression profile of OPA1 protein forms in different tissues is summarised in the Table 4.4.

The total amount of mouse OPA1 protein varied from tissue to tissue in relation to beta-actin (data not shown). Brain tissue showed the highest expression of OPA1 protein while liver contained the least amount of OPA1. In comparison to other tissues, these results indicate that the OPA1 protein isoform running at ~95-kDa (band-2) predominates in the brain tissue, which might be related to its particular function in the brain.

4.3 Identification of OPA1 protein isoforms

The mouse OPA1 transcript analysis had revealed the presence of four different splice variants, while at least six different protein isoforms were present on western blots (see above). Moreover, the OPA1 protein expression pattern was tissue specific, although the distribution and intensity between different OPA1 isoforms was similar in the brain and retina in mice (Fig. 4.9).

In order to identify and correlate the OPA1 bands running at 75- to 95-kDa (1-5) with particular OPA1 isoforms in different mouse tissues (brain, heart, liver and kidney), OPA1 protein was immunoprecipitated from purified mitochondria using anti-OPA1 monoclonal antibody coupled to Sepharose beads, and the isolates were resolved on SDS-PAGE. The identity of different OPA1 bands was determined using ESI (electron spray ionisation) tandem MS/MS. Figure 4.11 represents the peptides identified for the N-terminal fragment containing first 320 amino acids of OPA1. The details on the peptides detected in MS/MS analysis are listed in the Chapter 7.4. All the identified peptides from different tissues were subsequently aligned to OPA1 isoform 8 (Chapter 7.4). The sequence coverage achieved in this MS study was 50-77% for each band.

The identities of different bands running at 72-kDa to 95-kDa were confirmed as OPA1 protein isoforms (Fig. 4.10). The peptides identified for bands-1 to -5 were analysed separately for each tissue. Band-4a and b were analysed together (Fig. 4.9). All five OPA1 bands were isolated and analysed in the heart and kidney, whereas only band-2 was examined in the brain. Bands-3, -4 and -5 were characterized in detail in the liver.

All bands (1 to 5) contained peptides that confirmed the presence of the OPA1 protein sequence corresponding to amino acids 270 (exon 6) to 1015 (carboxy terminal end) (Fig. 4.11). Certain peptides were particularly useful for distinguishing individual isoforms: 1) most N-terminal peptides, 2) peptides corresponding to alternatively spliced exons and 3) peptides bridging alternatively spliced exons. Only such peptides are mentioned below.

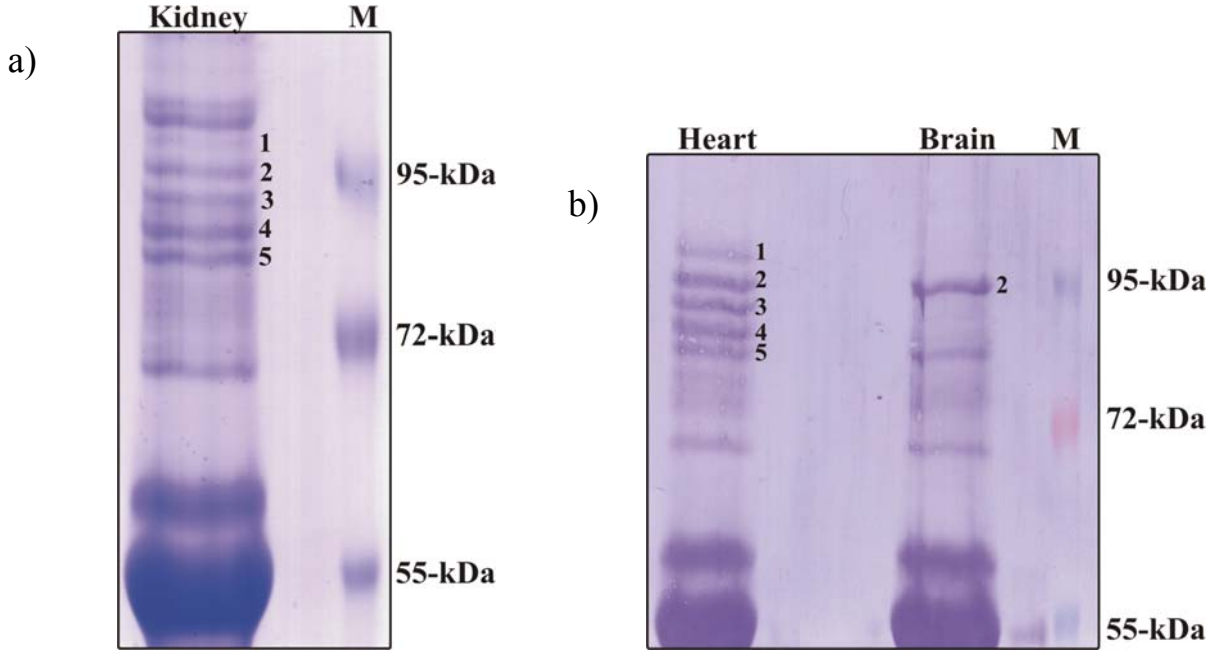

Figure 4.10: Immunoprecipitated OPA1 protein isoforms separated on SDS-PAGE.

a) OPA1 immunoprecipitated from purified mitochondria of different mouse tissues, using anti-OPA1 monoclonal antibody, were separated on 28 cm long 8% SDS-PAGE and the gel was stained with Imperial Protein stain. The identities of the OPA1 bands marked (1-5) were analyzed by mass spectrometry.

(b) OPA1 protein isoforms separated on SDS-PAGE were transferred on to PVDF membrane and the membrane was stained with Imperial Protein stain. The OPA1 bands marked (1-5) were processed for determining the N-terminal sequence using Edman degradation.

After trypsin digest of heart band-1, the most N-terminal peptide identified by MS started at amino acid position 102 corresponding to exon 2. Band-1 of heart also contained the peptides from exon 5b and a bridging peptide containing amino acids encoded by exon 4 and exon 5, but not exon 4b. This bridging peptide indicates the presence of an isoform translated from a transcript devoid of exon 4b. In the kidney, the band-1, the peptide bridging exons 4 and 5 and the peptide corresponding to exon 5b were also detected. In conclusion, band-1 must contain isoform 7 as exon 4b is absent and exon 5b is present.

Trypsin digest analysis of the brain band-2 revealed the same most N-terminal peptide as in the band-1, and the bridging peptide for exons 4/5. Unlike for band-1, no peptide was detected from exon 5b. The band-2, isolated from the brain and kidney were also analysed after Glu-C digestion by MS. The peptide “GLLGELILLQQQIQEHEEEA” was not detected thereby confirming the absence of exon 5b. Peptides derived from band-2 in all tissues were identical.

Figure 4.11: Alignment of the peptides identified from different bands to mouse OPA1 isoforms.

(++++) identified peptide with high ion score, (-) unidentified peptide in MS/MS analysis. The shaded region is the predicted transmembrane (TM) domain.

Henceforth, the absence of exons 4b and 5b revealed that band-2 contained OPA1 isoform 1. Also, the migratory size difference between band-1 and band-2, of ~4 kDa, agreed with the size difference of isoform 1 and 7 due to the protein sequence encoded by exon 5b (Fig. 4.10). The N-terminus of both isoform 1 and isoform 7 extends to amino acid position 102 (Fig. 4.11).

In the MS analysis after trypsin and Glu-C digest of kidney band-3, the peptides from exon 5 and 5b were detected, respectively. For the heart band-3 also peptides for exon 5b were identified. Liver band-3 contained only the peptides located downstream of exon 8. The low sequence coverage in the liver was probably due to the low amounts of OPA1 protein. Analysis of band-3 revealed the presence of exons 5 and 5b, but no peptides covering the region N-terminal to exon 5 were detected (Fig. 4.11). Thus, isoforms present in band-3 need to be processed N-terminally to amino acid 213 and contain a domain encoded by exon 5b.

Trypsin digest of band-4 detected one peptide (AAGQYSTSYAQQKR) corresponding to exon 5b. However, unlike band-3, neither Glu-C nor trypsin digests of kidney band-4 identified the peptide "GLLGELILLQQQIQEHEEEA" from exon 5b, although the quantity of protein in this band was sufficient for MS analysis. Peptides located N-terminally to exon 5b (aa 249) were not identified (Fig. 4.11). Therefore, isoforms identified in band-4 have to be processed between amino acids 230 and 249.

Trypsin digest analysis of band-5 revealed peptides located C-terminally (carboxy terminal) to amino acid 270. The analysis of Glu-C digested kidney band-5 confirmed this observation (Fig. 4.11). The amount of protein in this band should not limit the identification of peptides up-stream to amino acid 270. Therefore, isoforms present in band-5 appear to be the cleavage products after processing events immediately up-stream to amino acid 270.

In conclusion, although originating from different tissues, bands of the same size contained identical isoforms of OPA1. Bands-1 to -5 contained polypeptides, which varied in their N-terminal first 270 amino acids, but not in their C-termini. Isoform 7 and isoform 1 were clearly correlated to bands-1 and -2, respectively. In contrast, bands -3 and -4 seemed to contain proteolytically cleaved fragments of isoforms containing exon 5b. The polypeptide present in band-5 could have been generated from any isoform of OPA1.

4.3.1 Identification of the N-terminus of different isoforms of OPA1

The MS study provided internal protein sequence information but it was limited in revealing the exact N-terminus of the polypeptides present in each band. This information was important for the determination of the mitochondrial import cleavage site of OPA1 and for the determination of the exact sites used in post-translational processing of long OPA1 forms into

short ones. Therefore, it was decided to identify the exact N-termini for each of the different OPA1 protein isoforms by N-terminal microsequencing (Fig. 4.10b).

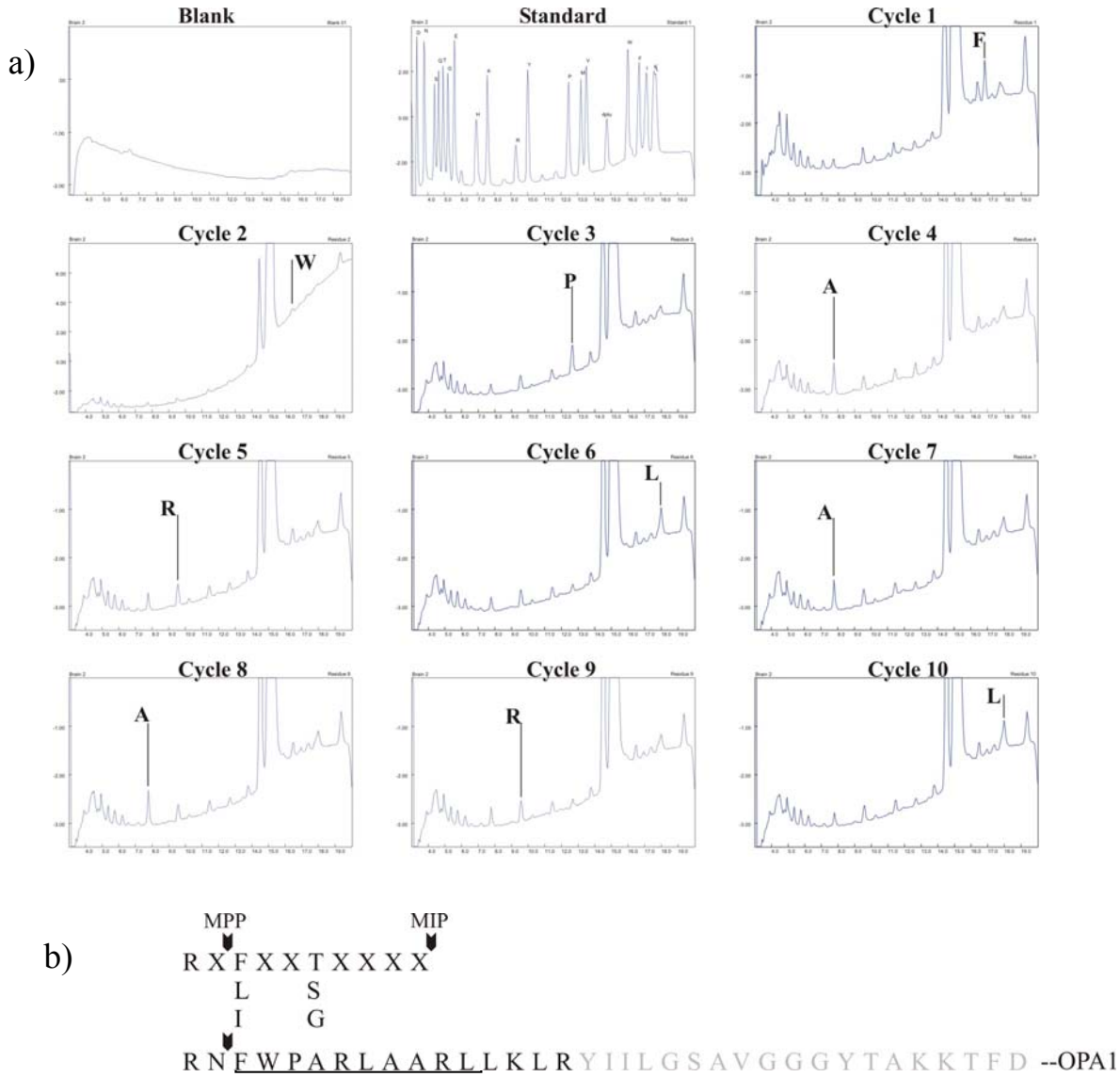

Figure 4.12: Edman sequencing of OPA1 isoform 1.

a) N-terminal protein microsequencing of isoform 1 from heart and brain tissues revealed the OPA1 sequence FWPARLAARL (aa 88-98 of OPA1).

b) The octapeptide recognised by MPP and MIP proteases. The sequence of OPA1, which is recognised by MPP protease, is depicted. The gray coloured amino acid sequence represents the peptide identified in MS analysis from band-2 (isoform 1). The N-terminal sequence of OPA1 isoform in band-2 is underlined.

The N-terminal sequence obtained for heart and brain band-2 was FWPARLAARL (Fig. 4.12a). This sequence corresponds to the amino acid positions 88 to 98 of OPA1. Therefore, one can conclude that OPA1 protein band-2 (isoform 1) starts at amino acid 88 and extends until the end of the C-terminus. Other OPA1 bands (3, 4 and 5) in the heart could not be sequenced though the quantity of the protein was not the limiting factor for the analysis. The most likely explanation for this is that the other OPA1 protein isoforms were blocked at the N-terminus. Unfortunately, 80-90% of the mammalian proteins are acetylated or otherwise

modified at their N-termini and, consequently, are resistant to Edman degradation (Hall et al., 1993).

Heart band-1 (isoform 7) could not be sequenced since the quantity of protein was below the threshold required for the analysis. However, one can speculate that the N-terminal sequence of both, isoforms 1 and 7 have to be identical, since their migratory size difference on SDS-PAGE could be attributed to the presence of exon 5b in the isoform 7. The proteolytic cleavage site at amino acid N87 of OPA1 is in agreement with the mitochondrial processing peptidase (MPP) cleavage motif, removing the mitochondrial targeting sequence during its import into the mitochondria (Fig. 4.12b).

Usually, the MPP cleavage is followed by a second proteolytic intervention mediated by the mitochondrial intermediate peptidase (MIP). This seems, however, not to be the case for the import of OPA1 protein. The determination of exact N-termini of the other bands of OPA1 (3, 4 and 5) requires further investigation. Locating the exact cleavage sites on these OPA1 isoforms will provide further insight into the identity of proteases involved in the processing of OPA1.

4.4 Membrane topology of mouse OPA1 protein isoforms

Other groups have shown that OPA1 isoforms exist as both membrane bound and soluble forms (Arnoult et al., 2005; Frezza et al., 2006). OPA1 is associated to the inner membrane of mitochondria through the predicted N-terminal transmembrane domain (TM) and the C-terminal part is directed into the inter membrane space. The MS analysis indicated the presence of shorter OPA1 isoforms without the TM domain. In order to study the membrane association of different OPA1 isoforms, isolated mitochondria were subjected to alkaline extraction. The proteins resistant to alkaline extraction are considered to be "integral membrane proteins" (Olson and Spizz, 1986).

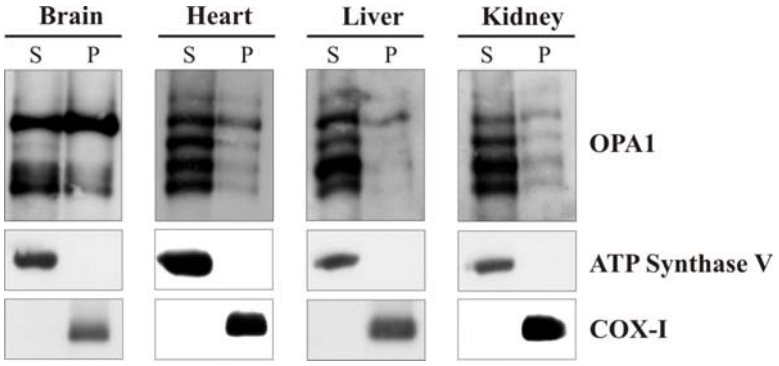

Figure 4.13: Membrane topology of mOPA1.

Western blot analysis of the TCA precipitated supernatants (S) and pellets (P) obtained after alkaline extraction (0.2 M Na_2CO_3; pH 13) with different antibodies OPA1 (1:5000), ATP synthase V (1:1000), Cox-I (1:500).

The transmembrane protein COX-I (subunit of respiratory complex IV) remained in the pellet, while the non-membrane F1 subunit of ATP synthase (respiratory complex V) was exclusively found in the supernatants. These proteins were used as controls to monitor the purity of the extracted fractions. It was observed that all isoforms of OPA1 were extracted into the supernatants. Only isoform 1 of OPA1 exhibited very tight membrane-association, which was predominantly observed in the brain and to lesser extent in heart and liver lysates. These results indicate that OPA1 is a type I membrane protein tightly associated to the mitochondrial inner membrane, especially in the brain and heart. All other isoforms of OPA1 are less strongly attached to the mitochondrial membrane (Fig. 4.13).

4.5 Complex forming property of the OPA1 isoforms

OPA1 belongs to the Dynamin protein family and analysis of its protein sequence by the "Pair Coils" program predicted the presence of two coiled-coil domains. Dynamin and Drp1 exist as tetramers, which have the potential to form very high molecular structures (Danino and Hinshaw, 2001). Mfn2 forms dimers via its C-terminal coiled-coil domains (Koshiba et al., 2004). The ability to form higher complexes, the presence of two coiled-coil domains and the accumulation of mutations in the C-terminal coiled-coil domain; these three features about OPA1 were the basis to characterize the complex formation properties of the protein.

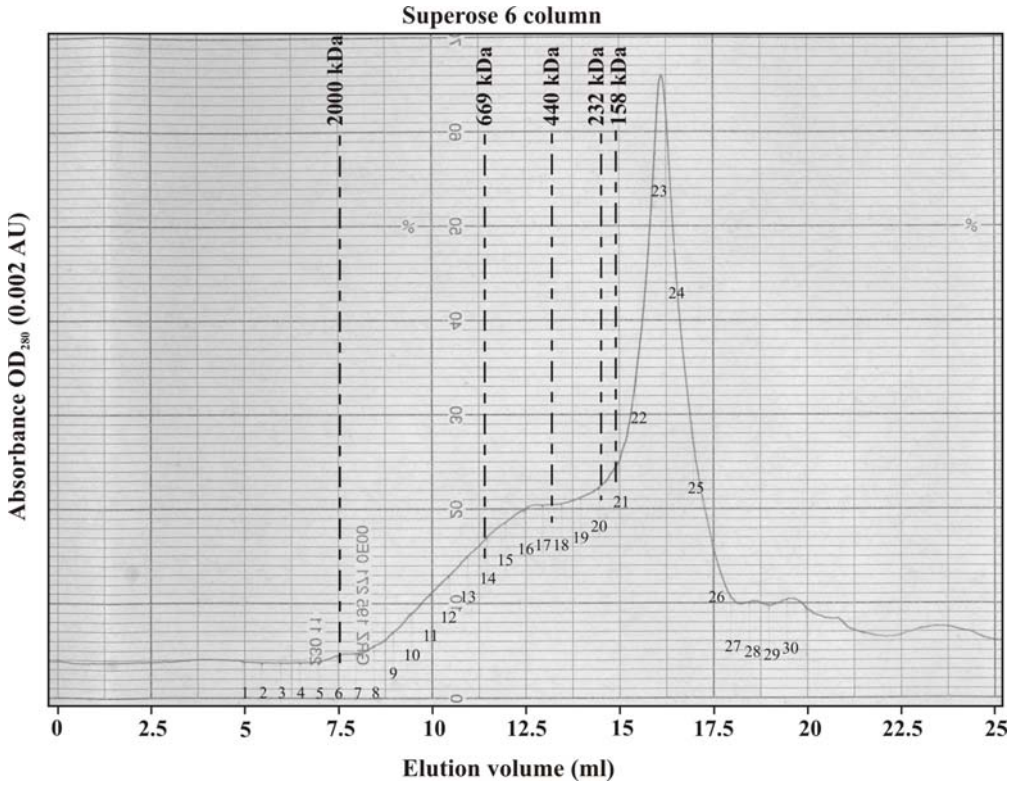

Figure 4.14: Elution profile of the mitochondrial lysates after gel filtration.
The above graph depicts typical elution profile for the mitochondrial lysates from each of the tissues analysed.

Single Dynamins have a molecular weight of ~100 kDa and form dimers and tetramers that can oligomerise into multimers *in vitro* (Shin et al., 1999). In accordance with these observations, OPA1 complexes were expected to have a size of 200 and 400-kDa. In order to properly separate mitochondrial protein complexes of that size, a Superose-6 column was used in size exclusion chromatography. The column was pre-calibrated with known protein standards in gel filtration running buffer and the equation $x = e^{[(y-1.1708)/(-0.1396)]}$ was deduced and utilized further to calculate the molecular mass of the eluted mitochondrial protein complexes (Chapter 3.8.3). Finally, the collected fractions were analysed on western blots after TCA precipitation.

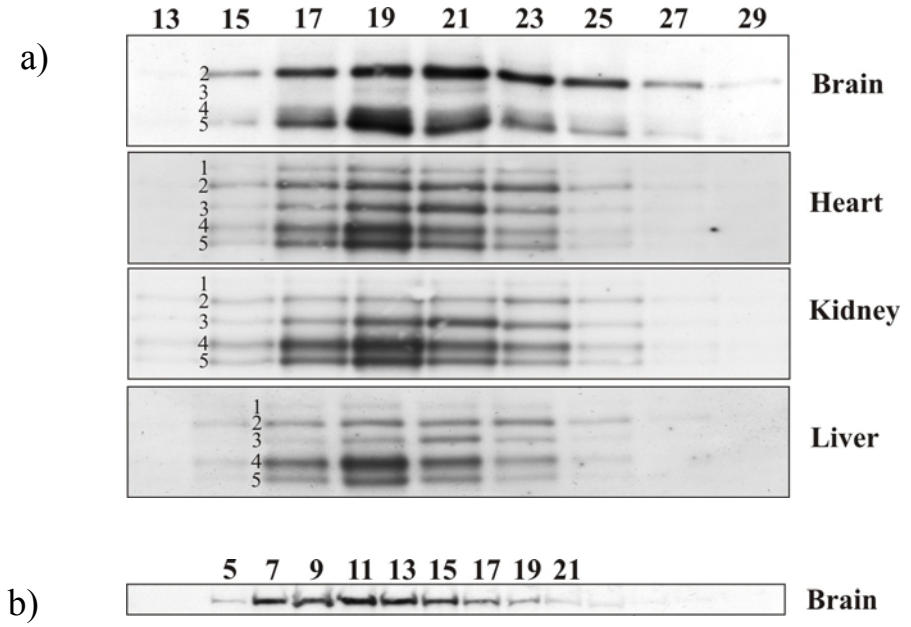

Figure 4.15: Western blot analysis of the TCA precipitated fractions after gel filtration.
Mitochondria isolated from mouse tissues (brain, heart, liver and kidney) were treated with 1% digitonin and applied to gel filtration column (Superose 6). (a) Blot developed with anti-OPA1 monoclonal antibody (1:5000). (b) Blot developed with anti-mitofilin monoclonal antibody (1:1000).

Table 4.5: Calculated mass of the protein complexes eluted in different fractions

Fraction no.	Elution volume (ml)	K_{av}	Calculated Mass (kDa)
13	10.875	0.1985	1058
15	11.875	0.2595	684
17	12.875	0.3206	441
19	13.875	0.3817	**285**
21	14.875	0.4427	**184**

The molecular mass of the protein complexes in different fractions was calculated based on the formulae deduced from standard curve (Fig. 3.2): $x = e^{[(y-1.1708)/(-0.1396)]}$; x = Molecular mass and y = K_{av}

The intensity of the OPA1 signal was the highest in fractions 19 and 21 (Fig. 4.15), which corresponded to the apparent molecular masses of 285-kDa and 184-kDa, respectively (Table 4.5). Thus, the ability of OPA1 to associate into high-molecular weight complexes was

confirmed. For each tissue, the signal strength of the individual OPA1 isoforms in the collected fractions was compared. Isoform-1 in band-2, bands-4 and -5 were mostly abundant in fraction 19, in all tissues (Fig. 4.16). The OPA1 isoform-7 in band-1 isolated from heart and liver was abundant in fraction 19, which was also observed for the brain and kidney after longer exposure of the ECL-film (data not shown). In contrast, the highest peak intensity for band-3 was observed in fraction 21, which was confirmed in all tissues (Fig. 4.16).

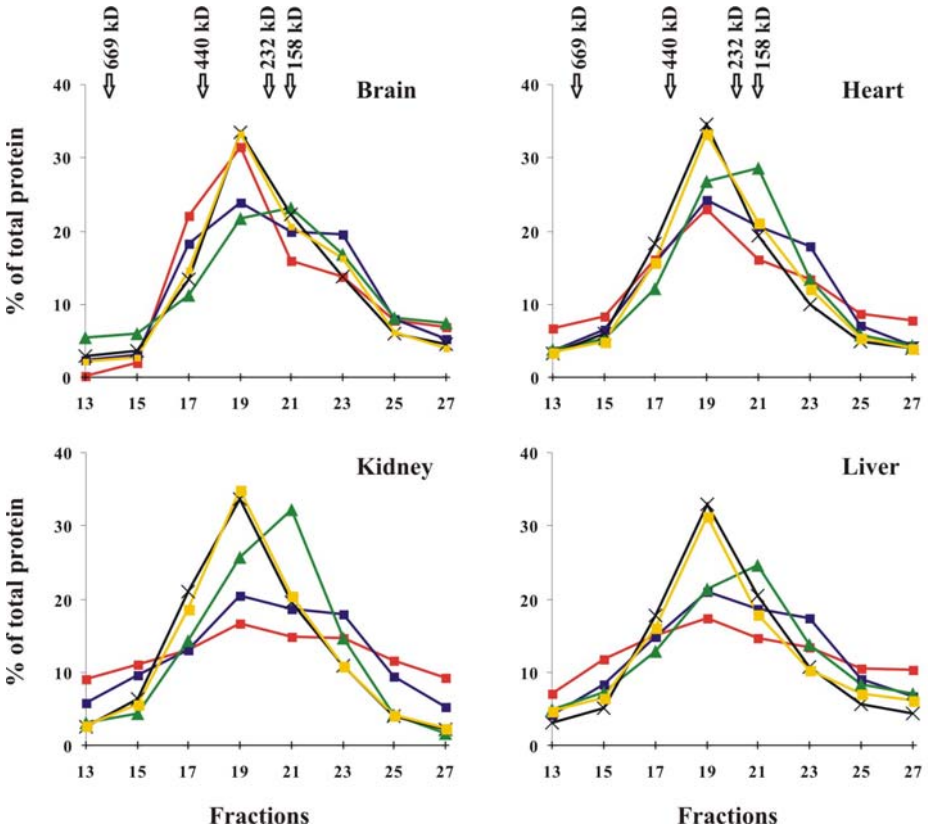

Figure 4.16: OPA1 isoforms build up different high molecular mass complexes.

The amount of OPA1 protein in each fraction from size exclusion chromatography was quantified using western blotting and densitometric analysis. The signal intensities of each OPA1 protein bands in different fractions *e.g.* Band 2 were calculated as 100% of immunoreactivity. The relative percentages of different isoforms of OPA1 are plotted for each fraction. Arrows indicate the position of marker proteins in size exclusion chromatography: aldolase 158-kDa; catalase 232-kDa; ferritin 440-kDa; thyroglobulin 669-kDa. Band 1; Band 2; Band 3; Band 4; Band 5.

In summary, isoform-7, isoform-1 as well as OPA1 isoforms present in bands-4 and -5 form higher molecular weight complexes at around 285-kDa (Fig. 4.16). Whether these isoforms combine into one heteromeric complex or oligomerise individually into homomeric complexes, remains to be elucidated. OPA1 isoforms represented by band-3 form the smaller complex of about 184-kDa (with the size of the monomer being ~90-kDa). Hence, it can be postulated that the 184-kDa complexes contain a dimer of this isoform.

Mitofilin was detected in co-immunoprecipitation experiments of OPA1 (Chapter 4.6.1). In order to test whether this protein was present in fractions 19 and 21, the TCA precipitated

fractions were analysed by western blot using anti-mitofilin monoclonal antibody. Mitofilin was not co-eluted with OPA1 isoforms. Instead, it was detected in a fraction with an apparent molecular mass of > 700-kDa (Fig. 4.15b).

4.5.1 Peptide array binding assay

The OPA1 protein consists of several protein domains that may contribute to the formation of higher complexes. The GTPase, the middle and the coiled-coil (CC) domains are common to all OPA1 isoforms eluted in fraction 19. Since coiled-coil domains are involved in oligomerisation and in dynamin self-assembly (Okamoto et al., 1999), the CC-I and CC-II domains of OPA1 became a major focus of assembly analysis. In order to determine the association properties of the CC domains, a peptide array binding-assay was established. The detailed methodology underlying this experiment was reported by Otte and co-workers (2003). Peptides were synthesized at Charité (Campus Benjamin Franklin, Berlin, Germany).

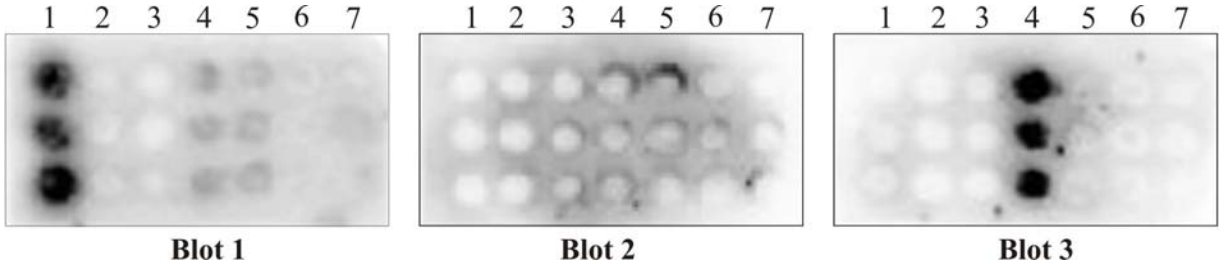

Figure 4.17: Peptide array binding assay.

Different peptides were synthesised and blotted on to a membrane in triplets and developed with biotinylated peptides from CC-I (blot-1), CC-IIa (blot-2) and CC-IIb (blot-3).

Lane 1- CC-I (211-254) SDKEKIDQLQEELLHTQLKYQRILERLEKENKELRKLVLQKDDKG
Lane 2- CC-IIa (895-920) RQQLTNTEVRRLEKNVKEVLEDFAED
Lane 3- CC-IIa (E907G) RQQLTNTEVRRLGKNVKEVLEDFAED
Lane 4- CC-IIb (923-960) KKIKLLTGKRVQLAEDLKKVREIQEKLDAFIEALHQEK
Lane 5- CC-IIb (924-fs1) KRLNCLLVNAFNWRKTSRKLEKFKKNLMLSLKLFIRRNKLKSYS
Lane 6- CC-IIb (924-fs2) EKFKKNLMLSLKLFIRRNKLKSYS
Lane 7- CC-IIb (924-fs3) KDAPKKNLMLSLKLFIRRNKLKSYS

In principle, peptides corresponding to CC-I (aa 211 to 254) and CC-II (aa 890 to 960) of OPA1 isoform 1 were synthesized and immobilised on cellulose membranes in an array of triplets via an N-terminal cysteine. Each of the membranes was incubated with biotinylated forms of the same peptides representing the OPA1 coiled-coil domains and developed with streptavidin-coupled alkaline phosphatase. The CC-II domain from 890 to 960 amino acids was synthesized as two peptides of 26 (CC-IIa) and 38 (CC-IIb) amino acids (Fig. 4.17). In addition, the influence of OPA1 mutations (previously identified in autosomal dominant optic atrophy patients) on the binding capacity of CC-IIa and CC-IIb was also assessed. Mutant peptides containing the E907G mutation in CC-IIa (Delettre et al., 2000), as well as a set of

frame-shift mutations in CC-IIb were compared with the wild type peptides (Delettre et al., 2000; Toomes et al., 2001).

CC-I and CC-IIb strongly self-associated without demonstrating any cross-reaction with other wild type or any mutated peptides (Fig. 4.17; blot-1). CC-IIa did not homo-associate or hetero-associate with CC-IIb (Fig. 4.17; blots 2 and 3). Peptides carrying frame-shift mutations in CC-IIb did not exhibit any binding (data not shown). In conclusion, CC-I and CC-IIb domains of OPA1 tend to strongly homo-interact, while CC-IIa does not self-associate although it was predicted, *in silico*, to form coiled coils. Mutations in CC-IIb abolish any interaction of this domain.

4.5.2 Sedimentation Equilibrium Analytical Ultracentrifugation

The peptide binding assay provides information on the qualitative binding of two peptides. Thus, although CC-I and CC-IIb showed self-association, predictions on the nature of their self-association, i.e. dimer, trimer formation or orientation of binding partners, could not be made. Henceforth, sedimentation equilibrium (SE) analytical ultracentrifugation was performed using the peptides that displayed homo-association the binding assays. The ultracentrifugation experiments were performed in collaboration with Dr. Holger Strauss (FMP-Berlin, Germany), and the details of the methodology are published by Beckman Instruments (Introduction to Analytical Ultracentrifugation by Greg Ralston).

Samples were run in 100 mM 2-Mercaptoethanol in PBS in order to reduce the disulfide bond formation between the N-terminal cysteines. The runs were performed at three speeds, 25,000; 35,000 and 50,000 rpm, and were continued (~18 h) until no significant difference in scans taken 2 h apart at 4°C was observed. At equilibrium, the solute distribution is invariant with time, so the measurement of the concentration at different points leads to the determination of the molecular weight of the sedimenting solute.

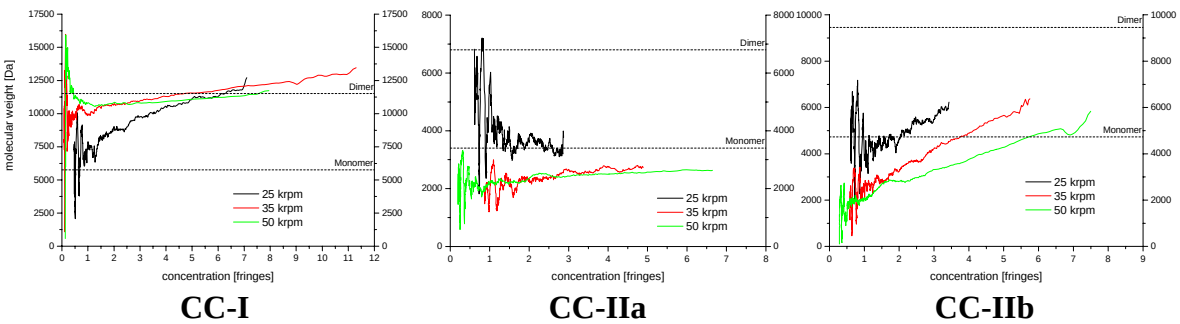

Figure 4.18: SE analytical ultracentrifugation.

Three peptides (CC-I, CC-IIa and CC-IIb) were analysed for association property by SE analytical ultracentrifugation at three different speeds.

Equilibrium ultracentrifugation of peptides CC-I, CC-IIa and CC-IIb revealed that CC-I was stably forming a dimer, while CC-IIb was present in equilibrium between monomer and dimer irrespective of the run speed (25, 35 and 50-krpm). The CC-IIa peptide did not show any association confirming the results of the peptide array binding assays. This strongly suggests that CC-I and CC-IIb are able to contribute to the homo-association of the OPA1 isoforms (Fig. 4.18). The peptides with mutations in CC-IIb and CC-IIa were not analysed, since they did not display any self-association in the peptide binding assays.

4.6 Identification of proteins interacting with OPA1

4.6.1 Search for OPA1 interaction partners by co-immunoprecipitation

Co-immunoprecipitation is a method of choice to identify stable protein-protein interactions. Therefore, proteins that co-precipitated with OPA1 during the immunoprecipitation using anti-OPA1 monoclonal antibody were identified by MS analysis. The proteins identified with this method included heat shock proteins (HSP60; *P63038* and HSP70; *P38647*), pyruvate carboxylase (*Q05920*), beta actin (*P60710*) and mitofilin (*Q8CAQ8*). Mitofilin is a mitochondrial protein localised in the inter membrane space involved in cristae remodelling (John et al., 2005). It was observed in size exclusion chromatography that mitofilin does not form a complex with OPA1 protein (Fig. 4.15). Therefore, it cannot be ruled out that the proteins, which co-immunoprecipitated with OPA1 are method contaminants.

4.6.2 Yeast Two-Hybrid screening

The Yeast Two-Hybrid (Y2H) system is a powerful tool for the identification of binary transient protein-protein interactions (PPI), which can be applied in high throughput manner to detect interactions across the entire proteome of an organism. To detect the proteins interacting with OPA1, the matrix library of human proteins was systematically screened using high throughput automated Y2H interaction mating (Stelzl et al., 2005).

Different regions of human OPA1 isoform 1 ORF (Fig. 4.19) were PCR amplified with specific primer pairs from the source clone 3F-1R-pCDNA and TA-cloned into pGEMT-Easy vector. The cloning was confirmed by restriction enzyme digest and sequencing. The bait and prey plasmids were generated by restriction cloning of these inserts into DNA binding domain and activation domain Y2H vectors (pGAD and pBTM). The details of the primers, Y2H plasmids and restriction sites used for cloning are provided in Chapter 7.2. The Y2H PPI study was performed by Dr. Ulrich Stelzl (AG Prof. Erich E. Wanker, Neuroproteomics, MDC, Berlin, Germany).

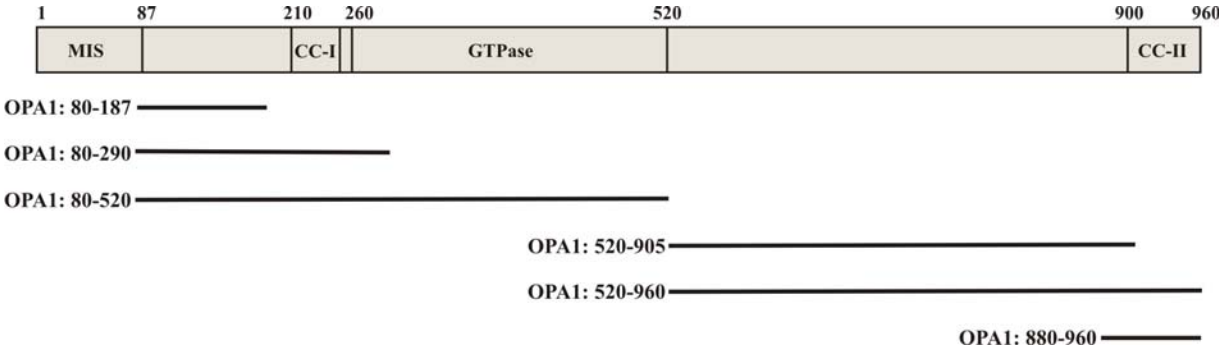

Figure 4.19: Schematic representation of the OPA1 regions amplified for the Y2H screen.
The numbers assigned to the clone name represent the amino acid position corresponding to the human OPA1 ORF isoform 1.

All six OPA1 baits did not auto-activate the reporter genes by themselves and were used in Y2H screens. The prey plasmids containing the OPA1 fragments under GAL4 activation domain were added to the matrix consisting of 5640 prey clones. Positive clones in the matrix mating, which activated the *HIS3* and *URA3* reporters, were identified by growth on selection plates and *lacZ* reporter gene activation in β-galactosidase assays. All positive preys identified in the first round of screening were individually retested for interactions with each of the baits in a second mating assay. An unambiguously positive interaction was only assigned to a pair of proteins after two independent mating assays (Stelzl et al., 2005).

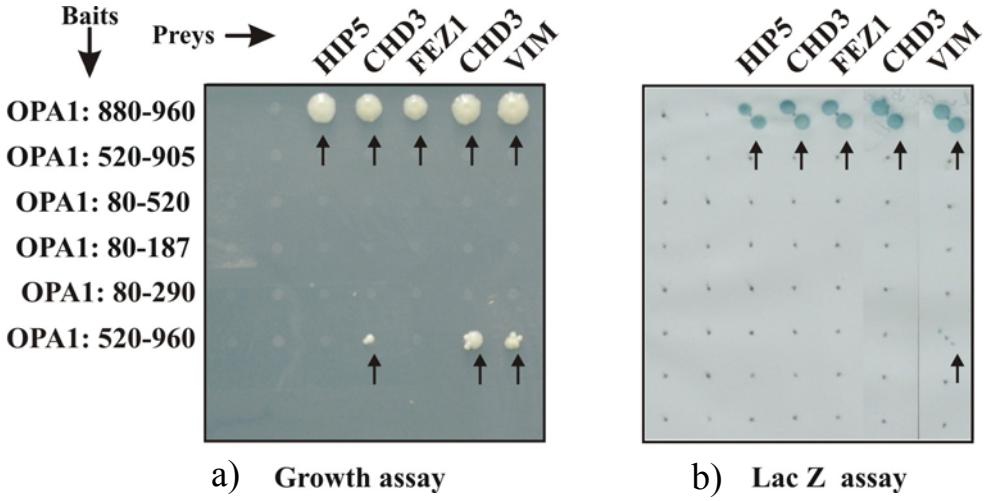

Figure 4.20: Identification of OPA1 interactions proteins by Y2H
a) Identification of Y2H PPIs using the pooled mating approach (first interaction mating). PPIs identified (arrows) by assaying the growth of diploid yeasts on SDIV (-Trp-Leu-His-Ura) agar plates.
b) Confirmation of Y2H interactions by analyzing yeast clones expressing single pairs of bait and prey proteins (second interaction mating). Diploid yeast clones were gridded in duplicates onto nylon membranes (3 × 3 pattern) placed on SDIV agar plates. Membranes were assayed for β-galactosidase activity to identify positive clones (arrows).

The Y2H matrix screen resulted in identification of four novel proteins, all of which interacted with the same bait protein (Fig. 4.20). Huntingtin interacting protein 5 (HIP5; KIAA1377), the Fasciculation and Elongation protein Zeta 1 (FEZ1), Chromodomain helicase

DNA binding protein 3(CHD3; 2 clones) and Vimentin (Vim) were identified to specifically interact with the C-terminal coiled-coil region (*OPA1: 880-960*) of OPA1 (Fig. 4.20a, b). VIM, FEZ1 and HIP5 were of interest because it was demonstrated that they interact with proteins involved in neurological diseases (Kuroda et al., 1999; Dubey et al., 2004; Morris et al 2003). The selected Y2H interactions were further validated by *in vitro* pull down assays.

Table 4.6: Details of the OPA1 interaction proteins

ID	Name	Locus ID	Accession	aa Match
HIP5	Huntingtin interacting protein 5	57562	Q9P2H0	445-988
FEZ1	Fasciculation and Elongation protein Zeta 1	9638	Q99689	131-392
CHD3	Chromodomain helicase DNA binding protein 3	1107	Q9Y4I0	1898-2055 1885-2055
Vim	Vimentin	7431	P08670	189-465

(Goehler et al., 2004)

4.6.3 In vitro pull-down assays

False positive interactions are known to frequently occur in Y2H assays (von Mering et al., 2002).

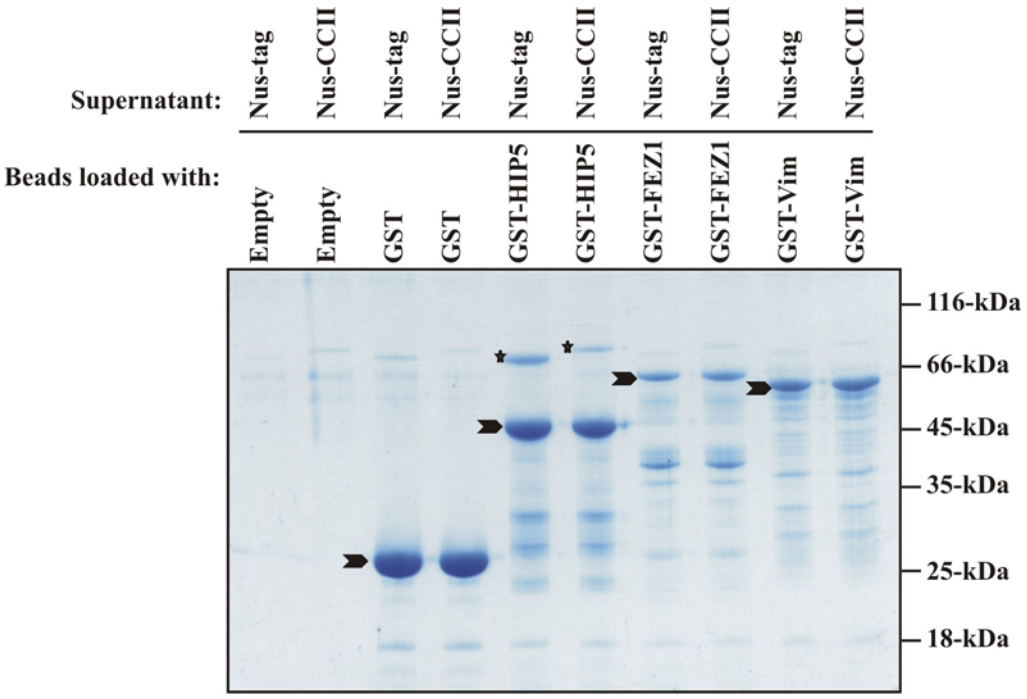

Figure 4.21: Confirmation of the interaction between OPA1 and selected proteins retrieved in the Y2H screen by *in vitro* pull-down assay.

In vitro pull-down assays between Nus-CCII (*OPA1: 880-960*) and the HIP5, FEZ1, and Vim proteins, all expressed as GST fusion proteins. Free GST control protein or the indicated GST fusion proteins were bound to glutathione-sepharose beads, washed and protein bound beads were incubated with the purified Nus-tag or Nus-CCII. After high stringency washes using binding buffer (20 mM HEPES pH 7.5; 300 mM NaCl; 5 mM EGTA; 6% glycerol; 0.25% digitonin; complete protease inhibitor) the samples was loaded in SDS-PAGE gels and stained with Coomassie blue. The arrows indicate the positions of the proteins listed above the lanes in the SDS-PAGE. * Indicate the positions of the Nus-Tag and Nus-CCII proteins.

In order to verify the interactions observed in the yeast two-hybrid assay, the three retrieved cDNA (HIP5, FEZ1, Vim) sequences were subcloned into bacterial expression vectors and expressed as GST-fusion proteins in E. coli (gift by Dr. Ulrich Stelzl). The bait (*OPA1: 880-960*) was subcloned by restriction cloning into pET-43.1a vector and expressed as Nus-OPA1-fusion (Nus-CCII) protein in E.coli. All four fusion constructs resulted in the expression of soluble proteins of expected sizes. A GST pull-down assay using glutathione agarose beads did not confirm the binding of Nus-CCII to the potential interaction partners (Fig. 4.21). Interaction between CHD3 protein and OPA1 is likely non-specific since CHD3 protein is a chromatin binding protein involved in chromatin assembly or disassembly. Thus, it was not used in GST-binding assay.

Failure to detect the interaction in GST pull-down assays could be either due to the lack of appropriate protein modifications or because the interaction between both proteins is transient in nature or a third partner is required for binding.